EPJ Web of Conferences **309**, 08003 (2024) https://doi.org/10.1051/epjconf/202430908003
EOSAM 2024

Frequency comb generation dynamics in $\chi^{(2)} + \chi^{(3)}$ AlGaAs microresonators

Francesco Rinaldo Talenti[1,2,*], *Luca* Lovisolo[1,2], *Andrea* Gerini[2], *Pedro* Parra-Rivas[3], *Tobias* Hansson[4], *Stefan* Wabnitz[4,5], *Laurent* Vivien[1], *Carlos* Alonso-Ramos[1], and *Giuseppe* Leo[2]

[1]Centre de Nanosciences et de Nanotechnologies, CNRS, Palaiseau, France.
[2]Université de Paris Cité, Laboratoire Matériaux et Phénomènes Quantiques, Paris, France.
[3]Sapienza University of Rome, DIET, Roma, Italy.
[4]Linköping University, Linköping, Sweden.
[5]CNR-INO, Istituto Nazionale di Ottica, Italy.

Abstract. We propose an AlGaAs microring resonator design for the generation of an optical frequency comb by means of the interplay between harmonic generation and Kerr effect. Modal phase matching imposes specific waveguide geometries and, consequently, it impacts the nonlinear efficiency of the system. We show the dynamics of $\chi^{(2)} + \chi^{(3)}$ comb generation resulting from type-I modal phase matching.

1 Introduction

Although optical frequency comb (OFC) generation has been demonstrated in purely quadratic or Kerr optical media, it remains largely unexplored in the presence of both $\chi^{(2)}$ and $\chi^{(3)}$ nonlinearities [1–3]. Their interplay may result in lower pump power thresholds [2] and unveil novel interesting physics and OFC soliton states. In this view, Aluminium Gallium Arsenide (AlGaAs) is interesting due to its high refractive index at telecom wavelengths (n = 3.28) and its huge nonlinearities (both quadratic and cubic) when compared with other common materials such as silicon nitride or lithium niobate. Moreover, the Aluminium molar fraction can be chosen in order to avoid two-photon absorption.

Optimized waveguide geometries for AlGaAs microresonators [4] has already led to record-low (μW) power threshold [5] Kerr-OFC generation. In this work, we investigate the additional exploitation of $\chi^{(2)}$ interactions in AlGaAs Kerr microrings. To this end, we simulate the excitation of nearly cubic OFC regime, with second harmonic generation (SHG) effects assisting the dynamics. Besides the desire for a prescribed group velocity dispersion, SHG also imposes stringent requirements on the waveguide cross-section, when considering mixed $\chi^{(2)} + \chi^{(3)}$ systems.

2 Second harmonic generation

Let us consider an $Al_{0.18}Ga_{0.82}As$ epitaxial layer waferbonded to silica (Fig. 1 a). Typical waveguide cross sections for optimal dispersion profile in Kerr-OFC generation require a ridge with height $h \sim 400$ nm and width $w \sim 600$ nm [4, 5]. To understand if this configuration can also result in efficient SHG, we look for modal phase matching between the guided modes at ω_0 (fundamental frequency, FF) and $2\omega_0$ (second harmonic, SH) . We thus sweep the parameter w, while keeping h fixed, and compute the effective index n_{eff} of such modes (see Fig. 1 b). We find two different phase-matched configurations: 1) type-I, at $w \sim 610$ nm, between the TM_{00} mode at $\lambda_{\text{FF}} = 1.55$ μm and the TE_{02} mode at $\lambda_{\text{SH}} = 0.775$ μm, respectively [6, 7]; 2) type-II, at $w \sim 470$ nm, involving also the TE_{00} mode at λ_{FF} [8]. The SHG efficiency $|\kappa|^2$ is computed form the following [6]:

$$\kappa = \frac{\omega_0 \epsilon_0}{2} \int_S \chi^{(2)}_{xyz} e^{*x}_{\text{SH}} e^{y}_{\text{FF1}} e^{z}_{\text{FF2}} \mathrm{d}S \quad . \tag{1}$$

Here, we make use of Einstein's summation convention and consider a usual normalization N following the Lorentz reciprocity ($N = \frac{1}{2}\int e \times h^* \cdot \hat{z} dS$), where S is the waveguide cross-section and e,h are the electric and magnetic transverse field distributions. Due to the 3D-tensorial nature of $\chi^{(2)}$, $|\kappa|^2$ crucially depends on the orientation of the propagation direction with respect to the crystalline axes. In Fig. 1 c, θ is the angle of the propagation direction in the (001) plane with respect to the [100] axis. The plotted SHG efficiencies represent the two points of modal phase matching found by considering a straight waveguide. A ring configuration imposes a further requirement that defines the set of parameters $\{R, \lambda\}$, where $L = 2\pi R$ is the ring length and λ is the pump wavelength. This comes from the quasi-phase-matching (QPM) condition on the azimuthal mode-number m of the propagating fields, i.e. $\Delta m \equiv 2m_{FF} - m_{SH} = \pm 2$ [9]. In our case, the type-II QPM condition is fulfilled, at $\lambda_{\text{FF}} = 1.55$ μm, for waveguide widths $w = 466$ nm and $w = 477$ nm, while for type-I $w = 590$ nm and $w = 630$ nm. Next, we simulate the resulting OFC dynamics of a realistic ring resonator with the effective dispersion profiles reported in Fig. 1 d,e.

*e-mail: francesco-rinaldo.talenti@universite-paris-saclay.fr

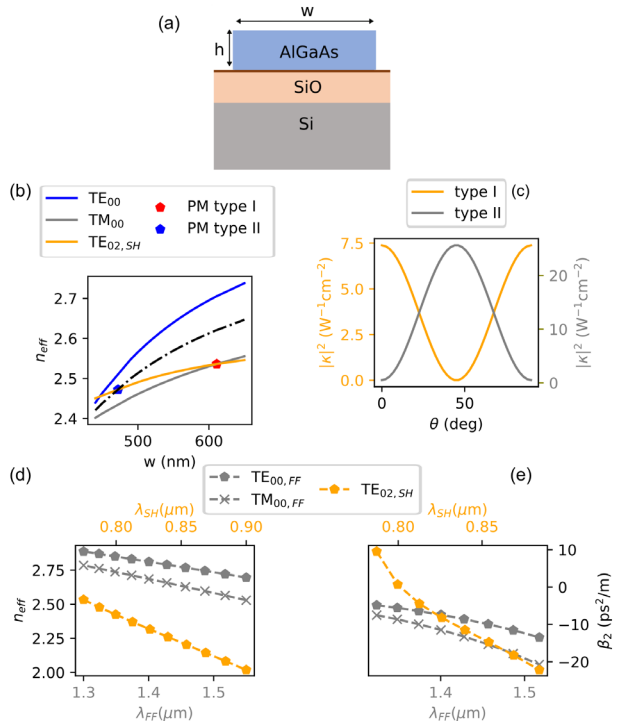

Figure 1. (a) Waveguide cross-section. (b) Modal phase matching between TE_{00} (blue) and TM_{00} (grey) at $\lambda_{FF} = 1.55\ \mu$m and the TE_{02} (orange) at $\lambda_{SH} = 0.775\ \mu$m. The black dashed line is the mean value of the two dispersion curves at λ_{FF}. (c) SHG efficiency for the two modal-phase-matching types of panel (b). (d) Effective index and (e) group velocity dispersion for $w = 600$ nm.

3 Frequency comb dynamics

The model used for our simulations is the same as in Ref.[1]. In our case, though, we use the full chromatic dispersion profile of the AlGaAs waveguide introduced above. The overall contribution of the $k^{\text{th}} \geq 2$ order dispersion terms β_k is evaluated in the Fourier domain by the following substitution:

$$FT\left\{\sum_{k\geq 2}^{\infty}\frac{\beta_k}{k!}\left(\frac{i\partial}{\partial\tau}\right)^k\right\} = \tilde{\beta}_0 + \tilde{\beta}_1(\omega-\omega_0) - \tilde{\beta}, \qquad (2)$$

where $\tilde{\beta}$ is the propagation constant, $\tilde{\beta}_k = \left(\partial^k\tilde{\beta}/\partial\omega^k\right)_{\omega=\omega_0}$ and the symbol $FT\{\cdot\}$ indicates the Fourier Transform operation. We then calculate the effective Kerr nonlinearity $\gamma = n_2\omega/(cA_{\text{eff}})$, for both cross- and self-phase modulation. Here, $n_2 = 2.6\times10^{17}\text{m}^2/\text{W}$ is the nonlinear refractive index of AlGaAs [4], while $A_{\text{eff}} = \int_S |e_i|^2 dS \int_S |e_j|^2 \text{d}S / \int_S |e_i|^2|e_j|^2 \text{d}S$ is the effective interaction area between the modes e_i and e_j. We consider optical losses $\alpha = 5\ \text{dBcm}^{-1}$, around both λ_{FF} and λ_{SH}, and critical coupling η, i.e. $\eta = \alpha L$. In our simulations we sweep the cavity by linearly increasing the laser-cavity detuning δ_0, and we suppose 0.1 W of CW input power at $\lambda_{FF} = 1.55\ \mu$m. The emerging nonlinear frequency mixing and comb generation dynamics is presented in Fig. 2. In panel (a) we report the intracavity energy of the FF and SH fields as a function of a normalized detuning $\Delta \equiv \delta_0/\alpha$, while in panels (b,d) and (c,e) we report two snapshots of the temporal and spectral dynamics, respectively, for two different values of Δ.

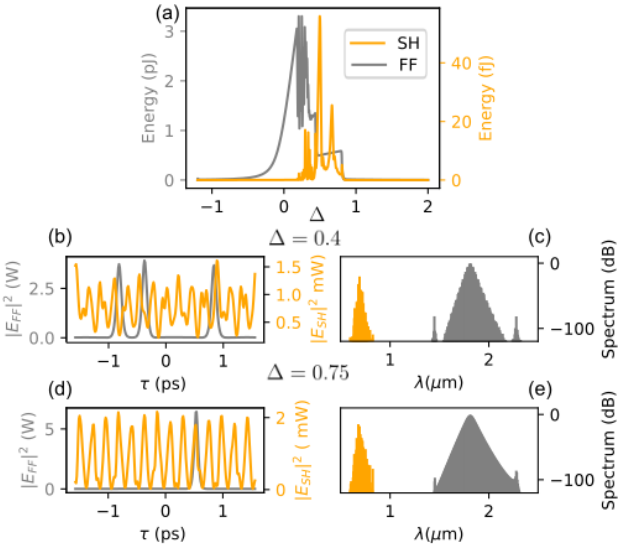

Figure 2. Frequency comb generation dynamics. (a) Intracavity energy of FF (grey) and SH (orange) fields. Temporal (b),(d) and spectral (c),(e) intracavity field distribution.

4 Conclusions

We simulated comb generation dynamics resulting from the interplay of $\chi^{(2)}$ and $\chi^{(3)}$ effects in AlGaAs microresonators, by perturbing a microring configuration already exploited for record low power threshold Kerr-OFC [4, 5]. In this specific case, $\chi^{(2)}$ is drastically weaker with respect to $\chi^{(3)}$ nonlinear effects. This is due to a particularly steep dispersion profile around the SH spectral region. We are currently addressing the problem of dispersion engineering by considering photonic crystals geometries and local Bragg mirroring effects [10].

References

[1] Xue, X., et al., Light Sci. Appl. **6**, e16253 (2017).
[2] Szabados, J., et al., APL Photonics **5**, 116102 (2020).
[3] Villois, A., et al., Opt. Lett. **44**, 4443-4446 (2019).
[4] Pu, M. et al., Optica **3**(12), 823-826 (2016).
[5] Chang, L., et al., Nat. Commun. **11**, 1331 (2020).
[6] Ciret, C. et al., Opt. express, **28**, 31584-31593 (2020).
[7] Poulvellarie, N. et al., Phys. Rev. A **102**, 023521 (2020).
[8] Poulvellarie, N. et al., Opt. Lett. **46**, 1490-1493 (2021).
[9] Chang, L., et al., APL Photonics, **4**(3) 036103 (2019).
[10] Talenti, F. R., et al., Phys. Rev. A **106**, 023505 (2022).